Molding Photonic Boxes into Fluorescent Emitters by Direct Laser Writing

Christof P. Dietrich, Markus Karl, Jürgen Ohmer, Utz Fischer, Malte C. Gather,* and Sven Höfling*

There is a rapidly increasing interest in the photonics research community to develop methods for immediate and on-demand fabrication of complex photonic structures. This is motivated by a desire to tailor the properties of components like interconnects, waveguides or cavities to specific but varying requirements. Due to their versatility and flexibility, organic materials are highly promising candidates for achieving this goal and a number of fabrication methods such as direct laser writing by two-photon polymerization[1–3] or direct circuit printing[4] have been suggested and are now developing rapidly.

Biologically produced fluorescent proteins (FPs) represent a special class of organic emitter materials. Due to their unique molecular structure, which comprises a highly fluorescent chromophore unit surrounded by a protective molecular bumper (β-barrel),[5,6] the chromophores are well protected from their surrounding and FPs are largely immune to concentration quenching.[7] This has allowed demonstration of low threshold lasers[8–11] and more recently formation of exciton–polariton condensation at room temperature under nanosecond excitation.[12]

Here, we demonstrate an approach for direct on-demand writing of photonic structures in thin films of FPs. Our approach exploits the usually unwanted effect of photobleaching which occurs in organic emitters upon excitation with high power lasers. In addition to the local loss of fluorescence, the bleaching also induces a local change in refractive index of the active organic material which allows us to introduce in-plane spatial confinement and guiding of photons in the active organic layer. Based on this principle, we demonstrate stimulated emission in three-dimensionally confined photonic modes and achieve lasing thresholds one order of magnitude lower than in planar unstructured reference devices. As the active FP in our microcavities, we use tdTomato, a tandem dimer protein, in which each molecule is formed by four β-barrels, each containing a chromophore at its center. The four barrels are arranged in pairs connected by a linker. tdTomato is one of the most widely used FPs and due to its large absorption coefficient (138 000 M^{-1} cm^{-1}) and high fluorescence quantum yield (0.6)[13] it offers high brightness and has proven to be well suited to generate lasing.[7]

Figure 1a shows the fluorescence of a tdTomato thin film (thickness, 500 nm) on a glass substrate when excited by an optical parametric oscillator (OPO) system with 530 nm nanosecond pulses of light with increasing pulse energy (2 µm spot size). There is a clear linear increase of the fluorescence with increasing pump pulse energy over a range of more than four orders of magnitude (from 1 nJ to 10 µJ per pulse). This proves that tdTomato films offer excellent photostability in the range required for lasing from tdTomato (reported lasing thresholds range between 1 and 1000 nJ).[7] However, for excitation energies larger than 10 µJ, the excitation-dependent fluorescence flattens and above 30 µJ we observe a drastic reduction in fluorescence. This behavior indicates the onset of irreversible photochemical interactions between neighboring chromophores and with ambient oxygen, i.e., photobleaching. The process of photobleaching in fluorescent proteins is still not fully understood. However, theoretical work indicates that photoinduced reactions of the FPs with molecular oxygen lead to the decomposition of the chromophore.[14] By exceeding the excitation energy for photobleaching, chromophore units are locally destroyed which is expected to reduce the excitonic contribution to the refractive index of the material. As a result, the refractive index in the bleached region will be lower than in the surrounding part of the film (but only in the spectral region of the excitonic resonance). If such a local index shift occurs inside a planar microcavity, one would expect a spectral shift of the cavity resonances as a change in refractive index also affects the optical thickness of the cavity.[15]

To verify that direct laser writing can be used for local refractive index tuning, we sandwiched a tdTomato film with similar thickness as in Figure 1a between two dielectric mirrors to form a microcavity, using the lamination approach described in ref. [10]. The reflectivity spectrum of the dielectric mirrors is shown in Figure 1d, together with the absorption and emission spectra of tdTomato. The mirrors have a central design wavelength of 620 nm, which matches perfectly with the emission of tdTomato. The anticipated spectral range in which efficient stimulated emission, i.e., optical gain, occurs in tdTomato lies well within the mirror stop band (see the gray box in Figure 1d).[7] Note the gap between the tdTomato

Dr. C. P. Dietrich, Prof. S. Höfling
Technische Physik
Universität Würzburg, Am Hubland
97074 Würzburg, Germany
E-mail: christof.dietrich@physik.uni-wuerzburg.de
M. Karl, Prof. M. C. Gather
SUPA
School of Physics and Astronomy
University of St. Andrews, North Haugh
KY16 9SS St. Andrews, UK
E-mail: mcg6@st-andrews.ac.uk
J. Ohmer, Prof. U. Fischer
Institut für Biochemie
Universität Würzburg, Am Hubland
97074 Würzburg, Germany

DOI: 10.1002/adma.201605236

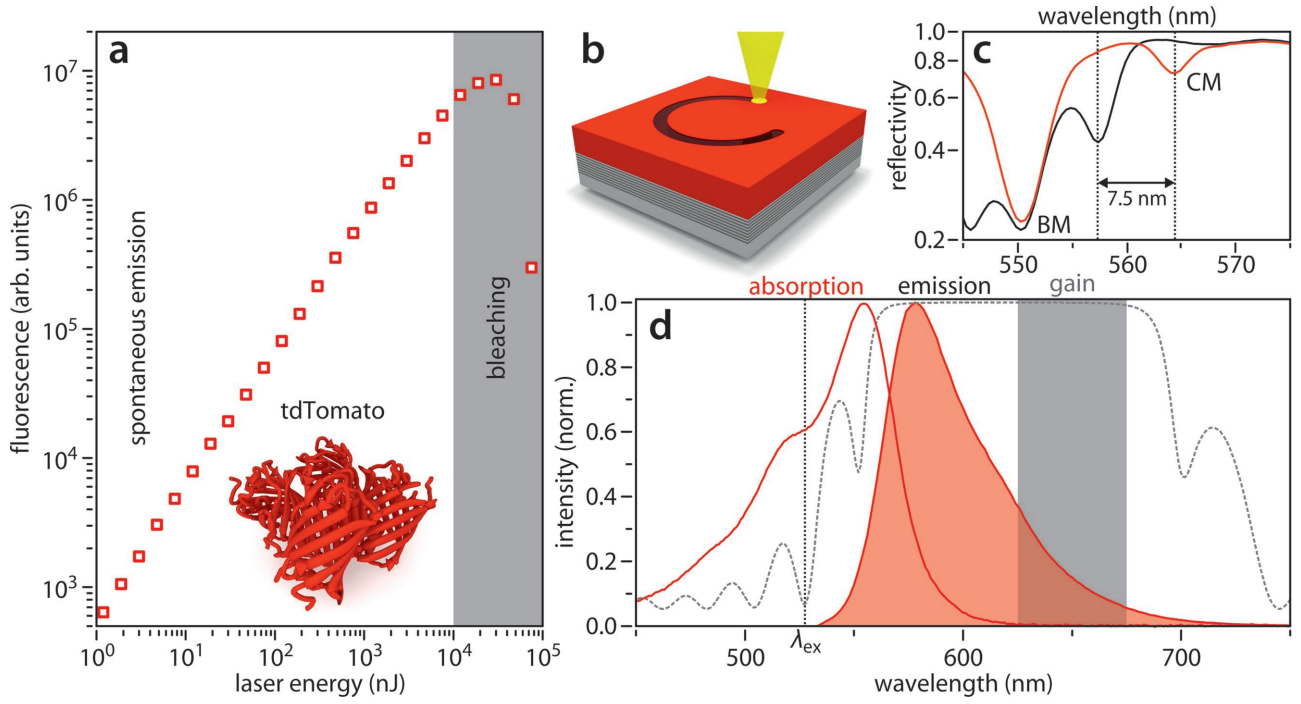

Figure 1. a) Fluorescence of a solid-state thin film of the fluorescent protein tdTomato (thickness, 500 nm) versus excitation pulse energy (excitation wavelength, 530 nm). The gray area marks the range in which photobleaching occurs. b) Illustration of laser-writing scheme using high energy laser pulses to adjust the refractive index of a protein film. c) Reflectivity of a protein filled microcavity before (red line) and after (black line) strong laser irradiation, showing a 7.5 nm shift of the cavity mode (CM) but no shift of the Bragg mode (BM). d) Absorption (red line) and emission (red shaded area) spectrum of tdTomato and reflectivity spectrum of the used distributed Bragg reflectors (gray dashed line). The gray area indicates the range of efficient stimulated emission (gain region) for tdTomato and the black dashed line marks the wavelength of the excitation pulses λ_{ex}.

emission maximum and the stimulated emission range which we attribute to optical losses induced by self-absorption.[10] We further emphasize that the peak of the absorption spectrum of tdTomato lies just outside the stop band of the dielectric mirror. Hence, we do not expect to observe strong light–matter interaction effects as was the case previously for similar microcavities filled with the protein eGFP where we optimized for strong spectral overlap between the protein absorption and the stop band of the dielectric mirror.[12]

When measuring the local reflectivity of the microcavity containing the unbleached protein film we observe distinct cavity resonances (cavity modes, CM; red line in Figure 1c). The quality factors of these modes range between 300 and 1000. Next, we locally exposed the microcavity to nanosecond pulses from an OPO laser system (wavelength, 530 nm) using pulse energies well above the bleaching threshold (≈30 µJ). When no fluorescence was detectable anymore, there was also a very pronounced spectral shift of the cavity resonance seen in the reflectivity measurements (compare black line in Figure 1c). By contrast, the first Bragg mode of the dielectric mirrors (BM, first reflectivity dip outside the mirror stop band) did not shift. This is consistent with a change of the optical path length (product of cavity thickness and refractive index) inside the cavity but no change to the dielectric mirrors. Shifts in resonance wavelength up to 10 nm were observed, which is equivalent to an energy shift of 40 meV. Assuming that the geometrical thickness of the microcavity has not changed during laser exposure, we deduce that the shift in wavelength is due to a change of the refractive index of the tdTomato film. Since the wavelength shift amounts to 1.8%, the laser-induced index change caused by photobleaching can be determined to be also 1.8%.

In a next step, we used the index alteration induced by local photobleaching to tailor the photonic potential landscape in a deterministic fashion and thus induce lateral guiding of photons in the tdTomato film. By defocusing the laser beam, i.e., by vertically translating the focus of the laser used for bleaching onto an imaginary point behind the sample, we created an excitation profile that is composed of several concentric rings (donut profile) with different diameters and a high intensity circle in the center. Exposing the tdTomato-filled microcavity to high energy pulses then directly imprinted the profile into the film. When imaged via bright-field microscopy, darker areas of the tdTomato film correspond to the exposed, bleached regions whereas the unbleached areas show as bright areas (**Figure 2**a). Subsequently, the pulsed laser used to write the photonic potential landscape was refocused and the film was exposed to moderate laser pulse energies (≈6 nJ) to excite fluorescence and potentially laser emission in the film. As shown in Figure 2b, fluorescence only appears in non-irradiated parts of the film. We also note that the emission from the tdTomato film shows an oscillatory behavior along the ring orbit, indicating formation of a standing wave laser mode within the ring. This is consistent with a 3D photonic confinement in the microcavity that supports the formation of zero-dimensional laser modes.

To study the impact of photonic confinement further, we performed hyperspectral imaging[16] of the microcavity emission at

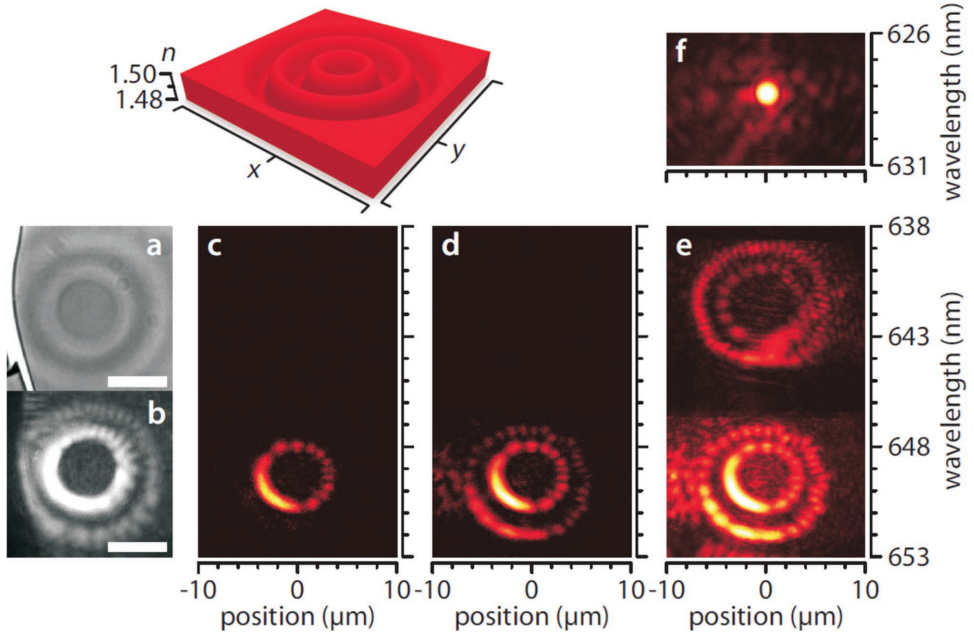

Figure 2. Top: Illustration of the estimated refractive index profile of the ring index trap formed in a thin film of tdTomato inside a microcavity. a) Bright-field image of the ring index trap. b) Real space image of emission from the trap inside a microcavity under excitation with 6 nJ laser pulses. Scale bar, 5 μm. c–e) Hyperspectral images of emission from the ring index trap for excitation pulse energies of 4 nJ (c), 6 nJ (d), and 8 nJ (e). f) Hyperspectral image of emission from an unstructured region of the tdTomato film within the microcavity.

different excitation pulse energies (Figure 2c–e). At low pump energies (≈4 nJ), emission is solely from the innermost index ring (Figure 2c). The circular shape of the refractive index trap promotes the formation of Laguerre–Gaussian modes (LGM, the solutions of the paraxial Helmholtz equation in cylindrical coordinates are Laguerre polynomials). Each LGM is described by its radial mode number p and its azimuthal mode number n. Due to the finite width of the ring, our structure preferentially supports modes with $p = 0$, the mode observed in Figure 2c has mode number $[n,p] = [8,0]$. The observed mode profile is slightly asymmetric which we attribute to unbalanced irradiation. When the excitation pulse energy was increased to ≈6 nJ (Figure 2d), we also observed emission from the outer ring, consistent with emission from a further cavity mode. In this case the mode azimuthal number was larger ([14,0]) which is a consequence of the increased mode volume. When increasing the pump energy even further (to ≈8 nJ), additional spectrally separated modes with a different longitudinal mode order appeared (Figure 2e).

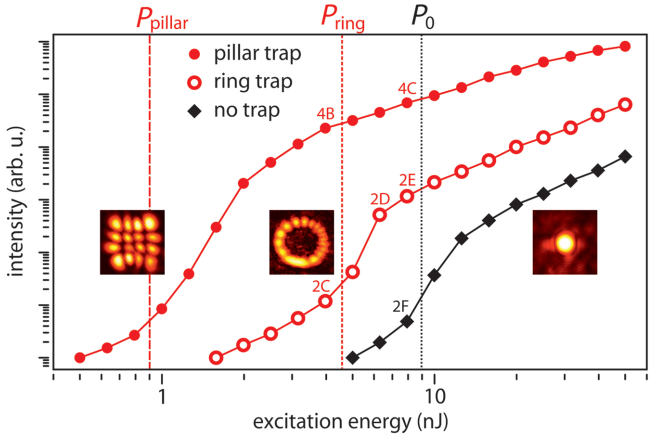

Figure 3. Input–output characteristics of the total emission intensity generated by a pillar-type trap (red filled circles), a ring index trap (red open circles), and for an unstructured thin film (black diamonds). The vertical lines denote the respective threshold energies for lasing in the different structures. Number/letter combinations at individual data points indicate the figure showing the respective emission pattern.

To confirm that the observed emission from the cavity indeed represents laser operation, we performed an excitation-dependent measurement of the integrated microcavity emission (open circles in **Figure 3**). The input–output characteristics show a pronounced S-shape behavior with the microcavity emission intensity entering a nonlinear regime when exceeding a certain threshold pump pulse energy. This characteristic is widely accepted as fingerprint for the presence of photon lasing. For the ring-shaped index trap, the lasing threshold was determined to be P_{ring} = 4.5 nJ. For comparison, we performed the same excitation-dependent measurement on an unbleached part of the sample (black diamonds in Figure 3). Like for the ring-like index trap, we again observed a clear threshold behavior, but the onset of lasing only occurred at a 2-fold higher pulse energy (P_0 = 9 nJ). We attribute this difference to the additional in-plane confinement provided by the ring trap which reduces photonic losses by suppressing leaky modes. This reduction in photonic loss apparently greatly surpasses any bleaching that may occur in the central spot of the excitation area during the process of writing the ring trap. In the absence of the ring trap, light is free to propagate within the protein film and away from the pump spot. The speckle pattern surrounding the central emission spot in the unstructured film is attributed to this leakage of photons (Figure 2f).

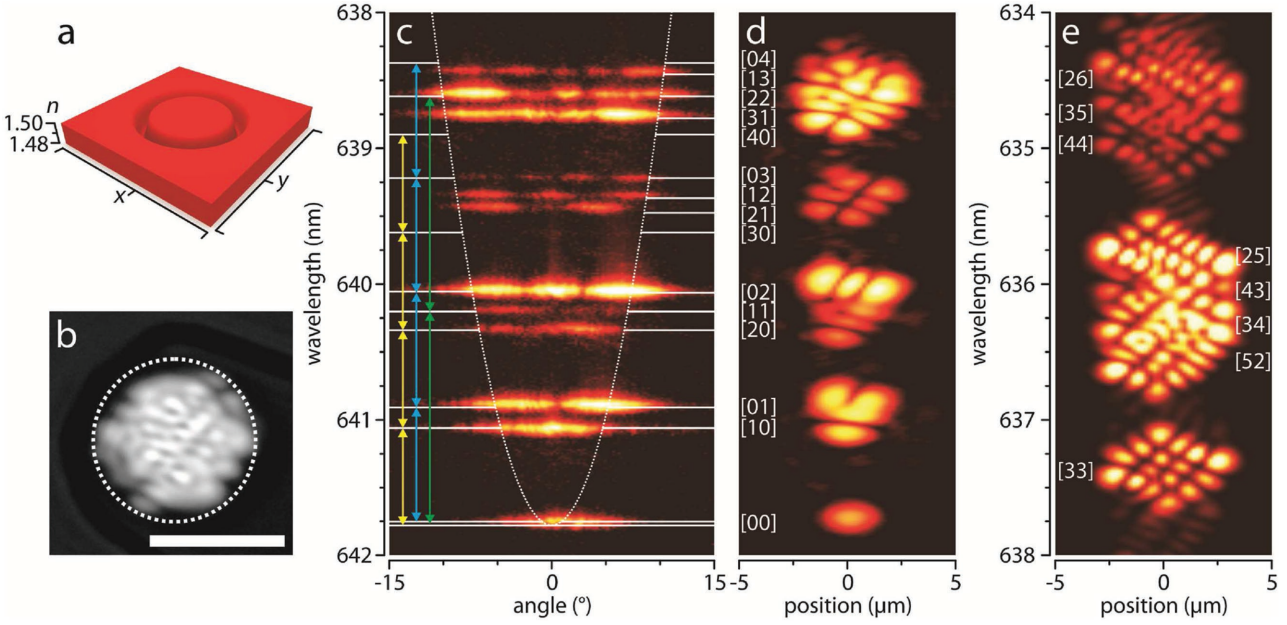

Figure 4. a) Illustration of the estimated refractive index distribution for the pillar-like index traps within a tdTomato film, formed by lateral translation of the sample. b) Real space image of the laser emission from the trap under excitation with 4 nJ pulses. Scale bar, 5 μm. c,d) Angle-resolved (c) and hyperspectral (d) emission images showing fundamental Hermite–Gaussian modes (HGM) in a circular index trap (with about 6 μm trap diameter). Numbers in square brackets give the respective HGM numbers l and m as [lm]. The vertical arrows indicate HGMs with $\Delta l = \pm 1$ and $\Delta m = 0$ (yellow), $\Delta l = 0$ and $\Delta m = \pm 1$ (blue), and $\Delta l = \pm 1$ and $\Delta m = \pm 1$ (green). Note that panels (c) and (d) use the same wavelength axis. e) Hyperspectral emission image of HGM with larger mode numbers for the same index trap.

Since vertical translation of the focus of the laser beam is limited to inscribing a particular photonic structure, we further performed writing experiments, in which the microcavity was translated laterally (within the sample plane) while being exposed to 30 μJ excitation pulses. By moving the sample in a circular manner, a pillar-like area of unbleached tdTomato was obtained (**Figure 4**a) which was then characterized by excitation with the same laser beam but at lower excitation energies (<100 nJ). For the pillar-like trap, the lasing threshold was reduced further compared to the circular trap, down to $P_{\text{pillar}} = 0.9$ nJ, which is one order of magnitude lower than P_0 obtained for the unstructured tdTomato film (Figure 3).

Like before, the emission pattern from the pillar-like trap shows signatures of photonic confinement (Figure 4b). However, instead of the circular modes confined to the rim of the trap that were observed previously, a complex mode pattern spreading over the entire pillar was observed. Hypothesizing that this pattern originates from a superposition of a multitude of simpler modes, we again applied hyperspectral imaging of the microcavity emission, this time in combination with Fourier imaging to also monitor the angular characteristics of the emission.[12] The spectrally and angle-resolved Fourier image of the microcavity emission (Figure 4c) reveals that indeed a variety of optical modes are confined within the photonic dispersion of the cavity resonance (indicated by white dashed line). All confined pillar modes were dispersionless. The corresponding spectrally resolved real space image of the pillar-like trap shows the mode patterns of the different confined pillar modes, ranging from the ground state mode with a circular pattern at the bottom of the photonic dispersion to more complex patterns at elevated energies (Figure 4d,e). Note that the mode patterns are rectangular rather than circular, indicating the presence of Hermite–Gaussian modes (HGMs) instead of LGMs. This is most probably caused by a slight refractive index anisotropy in the film or tilted mirror surfaces that induce a small but inherent rectangular symmetry to the pillar cavity.[17]

HGMs are the solutions of the paraxial Helmholtz equation in Cartesian coordinates and are typically labeled by two indices, l and m, which refer to the number of field minima along the two in-plane directions, i.e., the energetically lowest mode is labeled [00]. In Figure 4d,e we have labeled the majority of modes supported by the pillar-like trap with their respective mode number. In general, the resonance energy of the HGMs (LGMs) scales with the mode numbers l and m (n and p) due to the Gouy phase shift,[18] which becomes more pronounced as the lateral extension of the mode pattern increases. For HGMs the energetic difference between modes [l m] and [$l'm'$] is given by:

$$\Delta E(l,m,l',m') = \frac{hc\Delta\varphi}{2\pi d}\left[(l+m)-(l'+m')\right] \quad (1)$$

where d is the cavity thickness and $\Delta\varphi$ is the phase shift at the mirror/protein interfaces. Equation (1) unveils that the spectral shift between different HGMs directly scales with Δl and Δm. Experimentally, this is evidenced by a constant energy separation between modes differing by ±1 in l and/or m (differently colored vertical arrows in Figure 4c). For a perfect cylindrical resonator, the energy of all modes with equal values of $l + m$ should have the same energy.[19] However, this is not the case for our data as there are obvious energetic differences between, e.g., the [01] and [10] modes or the [20], [11] and

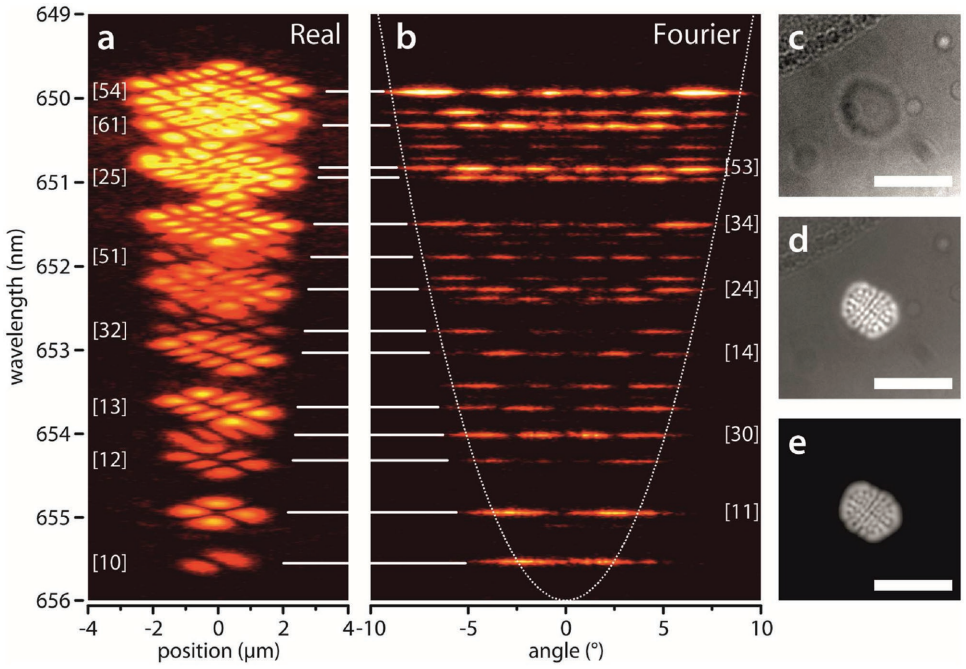

Figure 5. a,b) Hyperspectral (a) and angle-resolved (b) emission images for a slightly elliptical trap, showing fundamental HGMs. The numbers in square brackets give the respective HGM numbers. c–e) Bright-field (c), combined bright-field and laser-emission (d), and laser-emission (e) images of the trap. Scale bar: 5 μm.

[02] modes. We attribute these differences to a small amount of ellipticity in our pillar structure which lifts the mode degeneracy. The advantage of this effect is that different modes with equal $l + m$ values can still be spectrally resolved and imaged.

Our laser-writing technique can also be applied to create tailored photonic confinement potentials, e.g., a pillar-like index trap with a higher degree of ellipticity ($\varepsilon \approx 15\%$, see **Figure 5**c). This type of trap also supports stable laser modes with HGM profiles (Figure 5a,b). In contrast to the pillar-like trap discussed before, this structure predominantly supports HGMs with $l \neq m$ and these are preferentially aligned along the long elliptical axis while modes with $l = m$ are mostly suppressed, i.e., modes [00], [22], [33] etc. are absent.

In conclusion, we have demonstrated that by controlled bleaching of thin films of fluorescent protein it is possible to spatially tailor the photonic landscape in the active layer of a microcavity. Illumination with high energy laser pulses locally reduces the refractive index of the organic material, leading to stable confinement and guiding of photons in the non-exposed regions. As an example, we discuss the creation of a ring-shaped index trap and two pillar-like traps with circular and elliptical cross sections and discussed the Laguerre–Gaussian modes formed in protein rings and Hermite–Gaussian modes observed for protein pillars. For all structures and cavity modes, laser emission was observed, with lasing thresholds up to one order of magnitude lower than in the unstructured planar case.

While our initial demonstration used biologically produced fluorescent proteins as a materials platform, the approach should be readily transferable to a range of other organic emitter materials, in particular to thin films of organic semiconductors. In addition, the developed approach is compatible with standard ambient conditions. Our findings thus pave the way to a wide range of elaborated photonic environments or even photonic circuits. The direct laser-writing process allows highly selective spatial variation of the refractive index which has already enabled controlled guiding of photons within an active layer and the fabrication of highly efficient photon lasers with customized beam shapes. While we have demonstrated the creating of photonic traps with diameters in the range of 3–5 μm, our applied techniques can certainly be used to write smaller structures. In the context of strong light–matter interaction, the ability to pattern organic emitters with high fidelity can provide a room-temperature platform to investigate the propagation of polariton condensates along predefined trajectories. Such experiments have so far been limited to cryogenic temperatures[20] due to the marginal exciton binding energy of the inorganic semiconductors required for these studies so far.

Experimental Section

Protein Expression: The tandem dimer tdTomato was cloned between the BamHI and the HindIII site of a pET28-His6-SUMO1 vector.[21] For expression, the plasmid was transformed into *Escherichia coli* BL21(DE3) pLysS cells (Novagen) and cells were cultured in superbroth medium containing 25 μg mL^{-1} Kanamycin and 35 μg mL^{-1} Chloramphenicol. Cultures were grown at 37 °C to an OD600 of 0.5, cooled down to 25 °C, and induced with 1.0×10^{-3} M isopropyl β-D-1-thiogalactopyranoside for 18 h. Cells were harvested by centrifugation, resuspended in binding buffer (20×10^{-3} M HEPES–NaOH pH 8.0, 300×10^{-3} M NaCl, 5×10^{-3} M imidazole, and 5×10^{-3} M β-mercaptoethanol) containing protease inhibitors (10×10^{-6} M phenylmethane sulfonyl fluoride, 10×10^{-6} M (aminoethyl)benzenesulfonyl fluoride hydrocloride, 10×10^{-6} M Leupeptin, 1×10^{-6} M Pepstatin, 5 U mg^{-1} Aprotinin), and lysed by sonication. Following ultracentrifugation at 150 000*g* for 1 h at 4 °C, the cleared lysate was incubated with NiNTA-Sepharose

(Qiagen) in batch for 2 h at 4 °C. After washing with the binding buffer, bound proteins were eluted with the binding buffer containing 500×10^{-3} M imidazole. Protein-containing fractions were subsequently pooled, supplemented with the SUMO-specific protease SenP2 (protease:protein ratio of 1:1000)[20] and digested for 24 h at 4 °C. The digested sample was dialyzed against ddH_2O and passed over a Superdex200 column (GE Healthcare). Finally, tdTomato was eluted at a single peak and was concentrated to 150 mg mL^{-1}.

Microcavity Preparation: Concentrated solutions of tdTomato (≈50 µL) were spin-cast onto dielectric mirrors (distributed Bragg reflectors, surface roughness below $\lambda/10$) designed for peak reflectance ($R \geq 99.995\%$) at a wavelength of 620 nm and consisting of 14 pairs of alternating SiO_2 (107 nm)/Ta_2O_5 (73 nm) layers. The structure was capped with an identical mirror on top to form the laminated microcavity. Subsequently, the tdTomato solution dries out and leaves a solid film with a nearly constant thickness of around 500 nm. The theoretical quality factors of the photonic modes formed in these cavities reach up to $Q = 3000$. Thin films of tdTomato for fluorescence characterization were fabricated on glass substrates in the same manner as described above.

Fluorescence Spectroscopy: The protein microcavities were excited by an OPO system with 7 ns pulse length tuned to 530 nm (second Bragg minimum of the dielectric mirrors) through a microscope objective with NA = 0.55 and 40-fold magnification. The real space image of the microcavity emission was subsequently collected through the same objective, and imaged either onto a conventional CCD camera or onto the wide open entrance slit of a spectrograph that was equipped with a multichannel EMCCD detector. Using a wide open slit projects every transversal mode pattern to a point on the CCD. Note that this hyperspectral image is not a true spectrum. For Fourier imaging experiments, the Fourier image was relayed onto the entrance slit with narrow slit width (0.06 nm spectral resolution) by placing an additional lens with its focal point at the back focal plane of the objective. Microcavities were mounted on an *xyz*-translation stage. Laser writing was performed with a laser energy of 30 µJ and a repetition rate of 20 Hz until no notable fluorescence was detected on the CCD anymore. Fluorescence measurements (Figure 1A) and imaging experiments (Figure 2) were conducted at varying excitation energies (adjusted by a motor-controlled attenuator) with 1 Hz laser repetition rate.

Data and Materials Availability: The research data supporting this publication can be accessed at http://dx.doi.org/10.17630/598e9ccb-77a8-44e4-902f-aa05f4af643b. Additional data related to this publication may be requested from the authors.

Acknowledgements

The authors acknowledge financial support from the European Research Council Starting Grant ABLASE (ERC StG 640012), the Scottish Funding Council (via SUPA), and the European Union Marie Curie Career Integration Grant (PCIG12-GA-2012-334407). M.K. acknowledges funding from the EPSRC DTG (EP/M506631/1). S.H. gratefully acknowledges support from the Engineering and Physical Sciences Research Council through the "Hybrid Polaritonics" Program Grant (Project EP/M025330/1).

Received: September 28, 2016
Revised: December 9, 2016
Published online:

[1] J.-F. Ku, Q.-D. Chen, R. Zhang, H.-B. Sun, *Opt. Lett.* **2011**, *36*, 2871.
[2] J. Lin, Y. Xu, J. Song, B. Zeng, F. He, H. Xu, K. Sugioka, W. Fang, Y. Cheng, *Opt. Lett.* **2013**, *38*, 1458.
[3] G.-M. Parsanasab, M. Moshkani, A. Gharavi, *Opt. Express* **2015**, *23*, 8310.
[4] J. K. Hohmann, M. Renner, E. H. Waller, G. von Freymann, *Adv. Opt. Mater.* **2015**, *3*, 1488.
[5] F. Yang, L. G. Moss, G. N. Phillips, *Nat. Biotechnol.* **1996**, *14*, 1246.
[6] M. Ormo, A. B. Cubitt, K. Kallio, L. A. Gross, R. Y. Tsien, S. J. Remington, *Science* **1996**, *273*, 1392.
[7] M. C. Gather, S. H. Yun, *Nat. Commun.* **2014**, *5*, 5722.
[8] Q. Chen, M. Ritt, S. Sivaramakrishnan, Y. Sunc, X. Fan, *Lab Chip* **2014**, *14*, 4590.
[9] A. Jonas, M. Aas, Y. Karadag, S. Manioglu, S. Anand, D. McGloin, H. Bayraktar, A. Kiraz, *Lab Chip* **2014**, *14*, 3093.
[10] C. P. Dietrich, S. Höfling, M. C. Gather, *Appl. Phys. Lett.* **2014**, *105*, 233702.
[11] H. J. Oh, M. C. Gather, J. J. Song, S. H. Yun, *Opt. Express* **2014**, *22*, 31411.
[12] C. P. Dietrich, A. Steude, L. Tropf, M. Schubert, N. M. Kronenberg, K. Ostermann, S. Höfling, M. C. Gather, *Sci. Adv.* **2016**, *2*, e1600666.
[13] N. C. Shaner, P. A. Steinbach, R. Y. Tsien, *Nat. Methods* **2005**, *2*, 905.
[14] B. L. Grigorenko, A. V. Nemukhin, I. V. Polyakov, M. G. Khrenova, A. I. Krylov, *J. Phys. Chem. B* **2015**, *119*, 5444.
[15] A. Mischock, F. Lemke, C. Reinhardt, R. Brückner, A. A. Zakhidov, S. I. Hintschich, H. Fröb, V. G. Lyssenko, K. Leo, *Appl. Phys. Lett.* **2013**, *103*, 183302.
[16] M. C. Gather, S. H. Yun, *Nat. Photonics* **2011**, *5*, 406.
[17] A. E. Siegman, *Lasers*, University Science Books, Mill Valley, CA, USA, **1986**.
[18] S. Feng, H. G. Winful, *Opt. Lett.* **2001**, *26*, 485.
[19] B. A. Saleh, M. C. Teich, *Fundamentals of Photonics,* Wiley, Hoboken, NJ, USA **2007**.
[20] E. Wertz, L. Ferrier, D. D. Solnyshkov, R. Johne, D. Sanvitto, A. Lemaitre, I. Sagnes, R. Grousson, A. V. Kavokin, P. Senellart, G. Malpuech, J. Bloch, *Nat. Phys.* **2010**, *6*, 860.
[21] D. Reverter, C. D. Lima, *Structure* **2004**, *12*, 1519.